Separation of intrinsic dielectric and resistive electrode losses in ferroelectric capacitors at radio frequencies

M.P.J. Tiggelman[1], K. Reimann[2], M. Klee[3], J. Schmitz[1], R.J.E. Hueting[1], J. Liu[2], Y. Furukawa[2], R. Mauczock[3] and W. Keur[3]

[1] MESA+ Research Institute, Chair of Semiconductor Components, University of Twente, Enschede (NL)

[2] NXP Semiconductors, Eindhoven (NL)

[3] Philips Research, Eindhoven (NL)

Abstract— **To analyze the intrinsic dielectric performance of planar high-density capacitors at radio frequencies (RF), the dielectric losses need to be distinguished from the resistive electrode losses. The resistive losses of the electrodes at RF are de-embedded employing a linear regression procedure with partial compensation for distributed effects. We use tunable ferroelectric capacitors with a barium strontium titanate (BST) dielectric with an inner diameter $d \geq 8$ µm on a silicon substrate. The de-embedding of the electrode losses has been successfully performed utilizing 1-Port RF measurement data from of an Advantest R3767CG vector network analyzer (VNA) in the frequency range of 10 MHz – 8 GHz.**

***Index Terms*—ferroelectric, tunable capacitor, barium strontium titanate, high-k dielectric and de-embedding.**

I. INTRODUCTION

TO support the integration of an increasing amount of technologies in handheld applications, system area and cost can be reduced employing reconfigurable passive building blocks. Reconfigurable components are able to change the performance of an electronic circuit to make it more suited for a specified technology within an application. Examples of tunable electronic components are tunable MEMS inductor [1] and tunable capacitor technologies, e.g. RF MEMS [2], varactor diodes [3] and ferroelectric capacitors [4]. We optimize tunable ferroelectric capacitors on silicon for integration into microwave frequency agile applications that could comprise of e.g. tunable filters [5], matching networks [6] or phase shifters [7]. Tunable thin film metal-insulator-metal (MIM) *ferroelectric capacitors on silicon* have several advantages e.g. continuous tuning at relatively low voltages (typically $V_{dc} < 50$ V for a MIM capacitor), small area ($A < 60$ µm^2), low cost, high permittivity $\varepsilon_r = 100-1000$**,** high capacitance density (typically 1−20 nF/mm^2) and integrated decoupling.

A low loss tangent (high unloaded Q) is mandatory for components in passive RF circuits with no active feedback that could compensate for dissipative losses. The electrical performance at RF is assessed using metal-insulator-metal (MIM) test structures.

II. THE RF TEST STRUCTURES

The circular shaped MIM capacitors are made suited for ground-signal-ground (GSG) measurements at RF. Only the top electrode is patterned [8] as depicted in Figure 1. The center (signal) pad varies in diameter d down to as low as 8 µm.

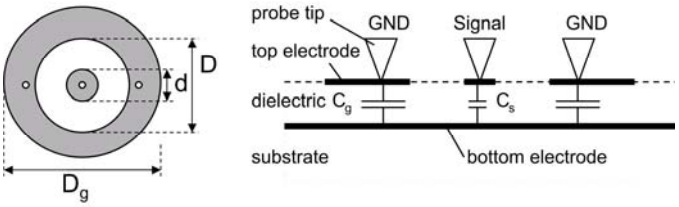

Figure 1. A top view of a MIM capacitor is given on the left side with white coloured landing spots for three probe tips of a single GSG probe. The cross-section is given on the right side.

The relatively small signal capacitance C_s is connected in series with the much larger ground capacitance C_g with an outer ring diameter of $D_g = 600$ µm and an opening of $D = 100$ µm. C_s is approximated by the equivalent series capacitance. The top electrodes consist of an Au/Pt stack and the homogeneous bottom electrode consists of Pt. The sheet resistance of the top electrodes is $R_{s,top} \approx 70$ mΩ/square and the sheet resistance of the bottom electrode is $R_{s,bottom} \approx 1.4$ Ω/square. A 110 nm thick BST dielectric, with a relative permittivity of $\varepsilon_r = 185$, is sandwiched in between the parallel metal plates.

III.MEASUREMENT SETUP AND CHARACTERIZATION

The test structures are measured at RF utilizing an Advantest R3767CG Vector Network Analyzer (VNA) from $f = 500$ kHz – 8 GHz with a single low contact resistance Infinity GSG probe (probe pitch = 125 µm). Preceding a short-open-load (SOL) calibration, with a load of $Z_0 = 50$ ohm and using built-

in routines, the magnitude and phase of the S_{11}-parameters are converted to Z_{11}-parameters [9] as expressed in

$$Z_{11} = Z_0 \frac{1+S_{11}}{1-S_{11}} = \frac{1}{Y_{11}} \tag{1}$$

An additional open measurement is performed to improve the low frequency performance of the smallest capacitors. The total Y_{11}-parameter

$$Y_{11,\mathrm{tot}} = Y_{11} - Y_{\mathrm{open}} \tag{2}$$

An R–C_s series circuit models the electrical behavior at RF with the equivalent series resistance R and the capacitor

$$C_{\mathrm{S}} = \frac{-1}{\omega \Im(Z_{11})} \tag{3}$$

To determine the capacitance density we have to take into account the area A according to the layout, the perimeter P, the stray fields, the dielectric thickness t and the undercut U of the capacitor plate. To determine the effective area

$$A_{\mathrm{eff}} = A + P\left(t\frac{2\ln(2)}{\pi} - U\right) \tag{4}$$

a conformal mapping technique [10] is employed to correct for stray fields in the dielectric.

All measurements were performed at zero DC bias, with an RF power P_{RF} = -10 dBm, without a bias-tee [11] and at room temperature.

III.1 DE-EMBEDDING OF THE ELECTRODES

The impedance parameters of the dielectric and the electrodes at RF have an immediate effect on the loss tangent. A de-embedding procedure of the electrode losses is required to separate the intrinsic dielectric losses from the resistive losses. The sum of the total loss tangent

$$\tan\delta = \frac{1}{Q} = \frac{\Re(Z_{11})}{|\Im(Z_{11})|} = \tan\delta_{\varepsilon} + \omega R C_{\mathrm{S}} \tag{5}$$

consists of the intrinsic dielectric loss $\tan\delta_\varepsilon$ and the resistive loss ωRC_s. For a lumped element case the resistance R is approximated by

$$R \approx R_{\mathrm{center}} + R_{\mathrm{ring}} + R_{\mathrm{outer}} + R_{\mathrm{contact}} \tag{6}$$

with [8,12]

$$R_{\mathrm{center}} = \frac{R_{\mathrm{S,top}} + R_{\mathrm{S,bottom}}}{8\pi} \approx \frac{R_{\mathrm{S,bottom}}}{8\pi} \tag{7}$$

with in our case a negligible small sheet resistance of the top electrode $R_{\mathrm{s,top}}$ compared to the sheet resistance of the bottom electrode $R_{\mathrm{s,bottom}}$. The resistance of the bottom electrode between the signal and the ground pad

$$R_{\mathrm{ring}} = \frac{R_{\mathrm{S,bottom}}}{2\pi}\ln\left(\frac{D}{d}\right) \tag{8}$$

and the connection to the ground probes R_{outer} can be neglected in most practical cases because of the larger diameter $D >> d$. The contact resistance of the GSG-probe in contact with an unpatterned top electrode surface yields R_{contact} = 0.1 Ω and is hence negligible.

The geometry factor of the electrodes (excluding $R_{\mathrm{s,bottom}}$)

$$g_{\mathrm{R}} = \frac{1}{8\pi} + \frac{1}{2\pi}\ln\left(\frac{D}{d}\right) = \frac{1}{2\pi}\left(\frac{1}{4} + \ln\left(\frac{D}{d}\right)\right) \tag{9}$$

and therefore the resistance

$$R \approx g_{\mathrm{R}} R_{\mathrm{S,bottom}} \,. \tag{10}$$

Before the de-embedding procedure we measure at least 3 capacitors with different inner circle diameters d. We performed measurements on capacitors with a dielectric thickness t = 110 nm and inner diameters of d = 8, 24 and 40 μm.

A lumped high-density capacitor becomes a distributed RC chain at RF. With an increasing RF the charge on the top electrode becomes more concentrated around the probe tip on the signal pad. Therefore, a voltage drop at the edges reduces the effective area of the capacitor and simultaneously reduces the capacitance value. Additional resistive losses are added onto the loss tangent. A high-density capacitor with a large physical size can transfer less charge across the top electrode with increasing RF due to the distributed nature of the capacitor. An increase in frequency will eventually reduce the capacitance and increase the resistive loss contribution. By plotting the loss tangent as a function of the measured C_s we partially compensate for distributed effects. The intrinsic dielectric loss tangent can be quickly visualized by a linear regression at f = 8 GHz to the intercept point on the y-axis ($C_s g_R$ = 0) as depicted in Figure 2. To determine the sheet resistance R_s the slope of one of the curves should be determined. The slope is equal to ωR_S. Depending on the starting point of the regression (d = 24 μm or d = 40 μm) R is estimated with frequency. The measured electrode losses can now be separated from the measured intrinsic dielectric losses with frequency using Eq.5. By de-embedding the resistive

electrode losses the measured intrinsic dielectric loss tangent can be obtained as depicted in Figure 3. This method overcompensates by deviating from the linear regression curve for *strong* distributed effects for relatively large physical size capacitors: lower C_s and high resistive losses (not shown). A deviation from the linear regression curve for capacitors with a small physical size would suggest the presence of process-induced edge damage (not visible in our data).

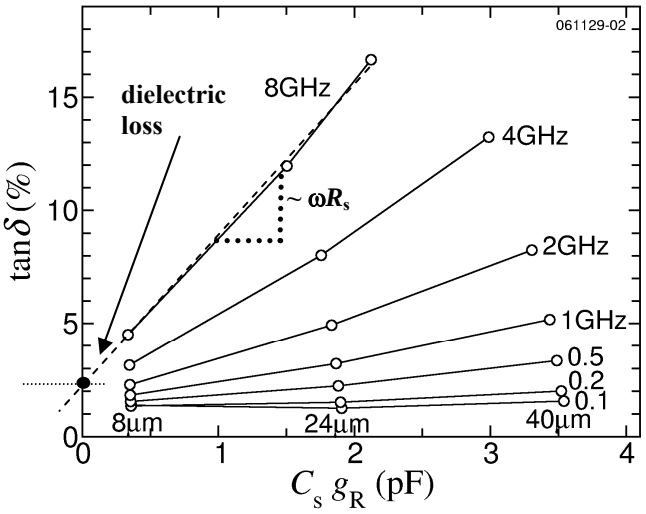

Figure 2. The intrinsic loss tangent can be separated using a linear regression. The slope of the curves is equal to ωR_s.

An intrinsic quality factor of $Q \cong 100$ at $f = 1$ GHz is achieved in Figure 3, which might be increased further with a DC bias.

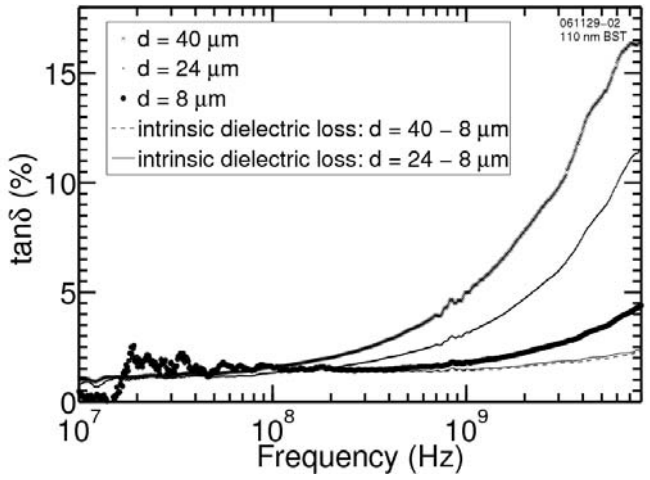

Figure 3. The total loss tangent tanδ of capacitors a BST dielectric with d = 8, 24 and 40 µm.

This easy-to-use, safe and fast de-embedding procedure gives the process engineer a clear picture on the extent of the intrinsic dielectric loss, how much the electrodes determine the quality factor at RF, if strong distributed effects are present for capacitors with large radii and if process-induced damage is present for the smallest capacitors.

IV. CONCLUSIONS

A regression-based procedure at RF is proposed, which enables the process engineer to get a swift overview on the intrinsic dielectric loss of high-density capacitors. The resistive loss contribution at RF caused by the electrodes is effectively separated from the (measured) intrinsic loss. The procedure *can* also indicate process-induced damage for capacitors with small radii and distributed effects for capacitors with large radii.

REFERENCES

[1] S. Chang and S. Sivoththaman, *A Tunable RF MEMS Inductor on Silicon Incorporating an Amorphous Silicon Bimorph in a Low-Temperature Process*, IEEE Electron Device Letters, vol. 27, no. 11, pp. 905–907, November 2006.

[2] Th.G.S.M. Rijks et al., *Microelectromechanical Tunable Capacitors forReconfigurable RF Architectures*, J. Micromech. Microeng., vol. 16, pp. 601–611, February 2006.

[3] K. Buisman et al., *Varactor Topologies for RF Adaptivity with Improved Power Handling and Linearity,* IEEE MTT-S Digest, pp**.** 319–322**,** June 2007.

[4] M. P. J. Tiggelman, K. Reimann, M. Klee, D. Beelen, W. Keur, J. Schmitz and R. J. E. Hueting, *Electrical Characterization of Thin Film Ferroelectric Capacitors*, Proceedings SAFE conference, November 2006.

[5] I. Vendik, O. Vendik, V. Pleskachev, A. Svishchev and R. Wördenweber, *Design of tunable ferroelectric filters with a constant fractional band width*, IEEE MTT-S Digest**,** vol.3, pp. 1461–1464, 2001.

[6] L.-Y. Vicki Chen, R. Forse, D. Chase, and R.A. York, *Analog Tunable Matching Network Using Integrated Thin-Film BST Capacitors,* IEEE MTT-S Digest, 2004.

[7] Q. Meng et al., *An Impedance Matched Phase Shifter using BST Thin Film,* IEEE Microwave and wireless components letters, vol 16, no. 6, June 2006.

[8] Z. Ma et al., *RF Measurement Technique for Characterizing Thin Dielectric Films*, IEEE Transactions on Electron Devices, vol. 45, no. 8, pp. 1811–1816 August 1998.

[9] D.A. Frickey, *Conversions Between S, Z, Y, h, ABCD, and T Parameters which are Valid forComplex Source and Load Impedances,* IEEE Transactions on Microwave Theory and Techniques, vol. 42, no.2, pp. 205–211, February 1994.

[10] S.B. Cohn, *Problems in Strip Transmission Lines*, IEEE Trans. on El. Devices, vol. 3, no. 2, pp. 119–126, March 1955.

[11] M.P.J. Tiggelman, K. Reimann and J. Schmitz**,** *Reducing AC impedance measurement errors caused by the DC voltage dependence of broadband high-voltage bias-tees*, IEEE Conference on Microelectronic Test Structures, pp. 200–205**,** March 2007.

[12] P. Rundqvist, A. Vorobiev, S. Gevorgian, and K. Khamchane, *Non-Destructive Microwave Characterization of Ferroelectric Films on Conductive Substrates*, Integrated Ferroelectrics, vol. 60, no. 1, pp. 1-19, February 2004.